

Magnon-polaron formation in XXZ quantum Heisenberg chainsD. Morais, F. A. B. F. de Moura, and W. S. Dias *Instituto de Física, Universidade Federal de Alagoas, 57072-900 Maceió, Alagoas, Brazil*

(Received 3 January 2021; accepted 14 May 2021; published 28 May 2021)

We study the formation of magnon-polaron excitations and the consequences of different timescales between the magnon and lattice dynamics. The spin-spin interactions along the one-dimensional lattice are ruled by a Heisenberg Hamiltonian in the anisotropic form XXZ, in which each spin exhibits a vibrational degree of freedom around its equilibrium position. By considering a magnetoelastic coupling as a linear function of the relative displacement between nearest-neighbor spins, results provide an original framework for achieving a hybridized magnon-polaron state. Such a state is characterized by high cooperation between the underlying excitations, where nondispersive profiles of the magnon wave function and the lattice deformations exhibit a bound dynamics. Traveling or stationary formation of a magnon-polaron depends on the effective magnetoelastic coupling, and the critical amount (χ_c) separating both regimes is shown. Different characteristic timescales of the magnon and the vibrational dynamics unveiled the threshold between such behaviors, as well as a limit value of critical magnetoelastic interaction, above which the magnon velocity no longer interferes at the critical magnetoelastic coupling capable of inducing the stationary regime.

DOI: [10.1103/PhysRevB.103.195445](https://doi.org/10.1103/PhysRevB.103.195445)**I. INTRODUCTION**

Collective excitations in the magnetic ordering of a material result in the well-known spin waves, the quanta of which are called magnons. The prospects of using magnons for wave-based computation and data transfer have been studied [1–5], and recent advances such as magnon transistors [1], spin-Hall oscillators [3], and spin-wave diodes [4] have been reported. Although magnonics is a promising approach [6,7], designing and controlling such quantum processes for long-time dynamics primarily requires an understanding of the role played by different ingredients.

Lattice vibrations are a key topic in condensed-matter physics, as they have remarkable effects on charge transport in polymers [8] and molecular crystals [9,10]. Although the first studies of the magnetoelastic coupling of magnons and lattice vibrations were performed some time ago [11–13], such aspects have been actively studied in both experimental [14–25] and theoretical frameworks [26–30]. Studies of magnetoelastic coupling in ferromagnetic manganese perovskites have shown that spin-wave softening and broadening are related to the nominal intersection of the magnon and optical phonon modes [14]. Experimental probing in ferrimagnetic insulators such as yttrium iron garnet (YIG) revealed evidence for the presence of magnon-phonon coupling [16], as well as the conversion of magnons into phonons with spin [17]. Nickel nanomagnet arrays were used experimentally to study the simultaneous formation of both elastic and magnetic modes; the results confirm that the coupling between the spin dynamics and the excited acoustic wave is responsible for the magnetic response of the system [18]. Signatures of the interaction between spin and phonon have been reported for magnetothermal transport measurements in *p*-doped Si [19],

as well as the layered semiconducting ferromagnetic compound CrSiTe₃ explored by Raman scattering experiments [20]. The magnon-phonon coupling and the formation of an optically excited magnon-polaron with high cooperation were described for a metallic ferromagnet with a nanoscale periodic surface pattern, where the symmetries of the localized magnon and phonon states have been reported as decisive for the hybridized state formation [21]. A strong coupling between magnons and phonons has been detected in the thermal conductivity of the antiferromagnet Cu₃TeO₆ [23]. Magnetic images have also shown skyrmions induced by propagating surface acoustic waves in multilayer films of Pt/Co/Ir [25].

From a theoretical point of view, magnetoelastic coupling has been theoretically studied to excite spin waves in magnetostrictive films through surface acoustic waves on piezoelectric substrates, in which driven spin waves were able to propagate up to 1200 μm [26]. Magnon-polaron excitations that exhibit magnon-phonon coupling controllable by the strength of the magnetic field gradient have been proposed for spin chains of arbitrary (anti)ferromagnets ruled by nearest-neighbor Heisenberg exchanges [28]. By using the coupled-mode theory, the conversion of an acoustic wave to a spin wave, as well as a backward conversion, were reported for a one-dimensional periodic structure (a so-called magphonic crystal) [29]. The problem of a two-dimensional antiferromagnet in the presence of magnetoelastic coupling was investigated in Ref. [30]. The authors demonstrate that the magnon and phonon bands are hybridized due to magnon-phonon coupling, with the properties of the magnon-phonon excitations suggesting a nontrivial SU(3) topology.

Another exciting experimental development involving the interaction between magnons and lattice vibrations was the spin Seebeck effect [31–33] and the bottleneck accumulation

of hybrid magnetoelastic bosons [34]. The former describes a spin current that appears in magnetic metal systems under the effect of a thermal gradient; this effect is enormously enhanced by nonequilibrium phonons [33]. The bottleneck accumulation phenomenon for a magnon-phonon gas demonstrates how magnon-phonon scattering can significantly modify the formation of a Bose-Einstein condensate of an ensemble of magnons, providing a novel condensation phenomenon with a spontaneous accumulation of hybrid magnetoelastic bosonic quasiparticles [34].

Previous studies have exemplified how the interaction between magnons and vibrational lattice modes became a hot topic of research. This interaction is considered to be a powerful method for spin control, and it can potentially be used as transduction from magnon signals to electrons [35]. With regard to the promising character of magnonics, we note the recent advent of advanced materials exhibiting high-frequency magnons, which has brought about the development of a new class of ultrafast spintronic devices [36–39]. Such studies have reported terahertz magnons in the two-dimensional (2D) Ising honeycomb ferromagnet CrI₃ [36], the ultrathin film of iron-palladium alloys [37], layered iron-cobalt magnonic crystals [38], and noncollinear magnetic bilayers [39]. As we consider all the previous aspects, we are faced with the following question: How does magnetic excitation behave under different timescales of the magnon and the lattice vibrations? In fact, the magnon excitation in a magnetoelastic lattice has an interdependent relaxation mechanism, and the formation of the magnon-polaron lacks a greater understanding. What would be the consequences of a spin transport that is as fast as the lattice dynamics?

To answer these questions, we offer a systematic investigation of a quantum Heisenberg model, in which each spin of a one-dimensional lattice exhibits a vibrational degree of freedom around its equilibrium position. Such character is described by a standard Hamiltonian of coupled harmonic oscillators, the magnetoelastic coupling of which is described by an exchange interaction that depends on the lattice deformations. By considering an intrinsic anisotropy-mediated magnetoelastic coupling, we explore the Heisenberg spin-spin coupling within an XXZ framework, the results of which demonstrate an original method for achieving a hybridized state referred to as a magnon-polaron. Such a state is characterized by high cooperativity between the underlying excitations, in which a traveling or stationary formation depends on the magnetoelastic interaction. We reveal the critical amount of the magnon-lattice interaction (χ_c) necessary for the emergence of the static magnon-polaron quasiparticle. Below the critical magnetoelastic interaction, the magnon-polaron excitation develops two fronts that propagate with constant velocity, with the spatial matching of their wave distributions exhibiting a selection of particular modes. Their velocities decrease continuously with the power-law dependence as the magnon-lattice interaction grows. By exploring the ratio between the characteristic timescales of the magnon and the vibrational lattice, we unveil a limit value of the critical magnetoelastic coupling, which is achieved as the magnon dynamics becomes much slower than the lattice dynamics.

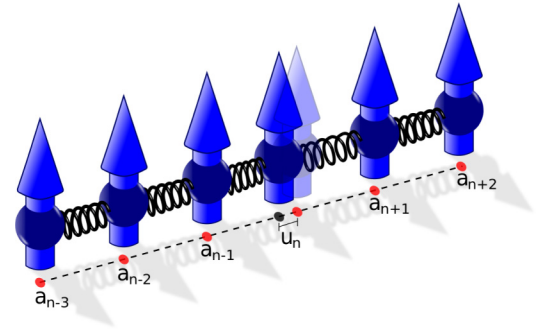


FIG. 1. Schematic drawing of the unidimensional spin lattice with effective harmonic springs coupling nearest-neighbor spins. The exchange interaction along the field direction ($J_{n,n+1}^Z$) is considered to be affected by the deviation of the spin from its equilibrium position (u_n). Thus, the magnetic excitation contributes to the emergence of vibrational components, the interaction of which is mediated by the magnetoelastic coupling that excites the magnon-polaron formation.

II. MODEL AND FORMALISM

The problem consists of analyzing a one-dimensional magnetoelastic lattice, in which spins $1/2$ are located at lattice sites (see Fig. 1). We consider an elastically isotropic crystal described by identical oscillators distributed along the lattice sites, which are ruled by a nearest-neighbor elastic coupling. Thus, the total Hamiltonian is comprised of magnetic and vibrational components,

$$H = H_{\text{mag}} + H_{\text{latt}}, \quad (1)$$

with the vibrational contribution of the system $\mathcal{H}_{\text{latt}}$ given by

$$\mathcal{H}_{\text{latt}} = \sum_n \frac{p_n^2}{2M} + \frac{\kappa}{2} (u_{n+1} - u_n)^2. \quad (2)$$

Here, M represents the mass of the ions, and κ is the effective spring constant. Further, $p_n = M\dot{u}_n$ describes the conjugated momentum for the n th spin. By considering the spin lattice along the x axis, we parametrize the Hamiltonian in terms of the displacement $u_n = a'_n - a_n$, with a'_n and a_n denoting the respective position and equilibrium position of ion n . We consider $\omega\hbar \ll k_B T$, in which $\omega = \sqrt{\kappa/M}$, k_B is the Boltzmann constant, and T is the temperature. In this framework, the lattice dynamics can be treated within the classical mechanics formalism.

The magnetic component is governed by a quantum Heisenberg Hamiltonian, in which the spin-spin interactions are described by a nearest-neighbor exchange. We study the XXZ model,

$$\begin{aligned} \mathcal{H}_{\text{mag}} = & E_0 + g\mu_B N H \\ & + \sum_n 2\hbar S (J_{n,n+1}^Z + J_{n,n-1}^Z) c_n^\dagger c_n \\ & - 2\hbar S J_{n,n+1}^{XY} c_{n+1}^\dagger c_n - 2\hbar S J_{n,n-1}^{XY} c_n^\dagger c_{n-1}, \end{aligned} \quad (3)$$

with $S = \hbar/2$, $J_{n,m}^Z$ denoting the exchange anisotropic component between the n th and m th spins, and $J_{n,m}^{XY}$ describing the exchange-coupling components in the XY plane. The ground-state energy in the presence of a uniform external magnetic

field is given by $E_0 = -g\mu_B N H S - S^2 \sum_n J_{n,n\pm 1}^Z$. Here, we will focus on the propagation of magnetic excitation. Thus, c_n^\dagger and c_n are, respectively, the creation and annihilation operators at the n th site. Whenever the creation operator is applied to the ground state, it leads to the excited state with the spin at site n flipped.

The underlying mechanism to magnetoelastic interaction is complex and needs further understanding, which has motivated theoretical and experimental studies. The magnetic anisotropy has been identified as being able to influence the dynamics of magnons arising at surface acoustic wave propagation in YIG films [40]. Recent experiments report the magnetoelastic interaction as strongly anisotropic and dependent on the direction of the external magnetic field [41,42]. On the other hand, exchange interactions between two neighboring spins depending on the interion distance have been experimentally evidenced [43,44], and they have been reported from an analytical and numerical study in bulk ferromagnetic insulators [45] and for the development of a Boltzmann transport theory of coupled magnon-phonon transport in ferromagnetic insulators [46]. Following the above scenarios, we consider an intrinsic anisotropy-mediated magnetoelastic coupling, such that the spin-spin coupling in the direction of the external magnetic field depends on the effective displacements between neighboring spins. We assume a regime of small-amplitude oscillations described by

$$\begin{aligned} J_{n,n+1}^Z &= J_0 + \alpha(u_{n+1} - u_n), \\ J_{n,n+1}^{XY} &= J_0, \end{aligned} \quad (4)$$

where α denotes the effective spin-lattice coupling affecting the longitudinal spin-spin interactions. Such a framework gives a ground-state energy ($E_0 = -g\mu_B N H S - S^2 N J_0$) that is independent of the vibrational modes of the spin chain.

We analyze two key parameters: (i) the effective coupling between magnetic properties and vibrational modes (i.e., the magnon-lattice interaction), $\chi = \hbar^2 \alpha^2 / J_0 \kappa$; and (ii) the ratio of the characteristic timescales of a magnon ($t_m = 1/\hbar J_0$) and an ionic chain ($t_l = 1/\omega$), written as $\tau = t_m/t_l$. The ground state of the system $|0\rangle$ is given by all spins pointing in the same direction, such that a spin deviation at a site n is described by $|n\rangle = S_n^- |0\rangle$. Thus, by employing the magnon wave function $|\Psi(t)\rangle = \sum_n \psi_n |n\rangle$ and a normalized spin position $x_n = \sqrt{\kappa/\hbar^2 J_0} u_n$, the set of equations that describe the dynamics of both magnon and lattice vibrations can be written, respectively, as

$$i t_m \dot{\psi}_n = 2\psi_n - \psi_{n+1} - \psi_{n-1} - \sqrt{\chi}(x_{n+1} - x_{n-1})\psi_n$$

and

$$\frac{t_m^2}{\tau^2} \ddot{x}_n = x_{n+1} + x_{n-1} - 2x_n - \sqrt{\chi}(|\psi_{n-1}|^2 - |\psi_{n+1}|^2). \quad (5)$$

The above set of differential equations was solved by using a standard Runge-Kutta method with a time step that is small enough to maintain the wave-function norm conservation ($|1 - \sum_n |\psi_n|^2| \leq 10^{-12}$) along the entire time interval considered. We concentrate our study by considering the initial state as a single spin flip fully localized and centered at rest in the static lattice center ($n = 0$ will be taken as the center of the chain). Such an initial state is a superposition of all

eigenstates within the allowed frequencies, including those less susceptible to the spread inhibitors [47–49]. The numerical integration was performed considering a self-expanding algorithm of the lattice size in order to avoid finite-size and border effects. Furthermore, we consider the characteristic timescale t_m as the relevant time unit. Ferromagnetic structures usually exhibit lattice dynamics with characteristic timescales on the order of picoseconds or shorter [21,22,50]. The magnon dynamics is typically slower (nanoseconds) [21,50,51], but recent materials displaying high-frequency magnons allow this range of timescales to extend to picoseconds [36–39]. Thus, we decided to investigate here the regime in which τ ranges from 1 to 100. Through the above-described procedure, we computed typical quantities that can provide information about the wave-packet time evolution, as will be detailed below.

III. RESULTS

Using the numerical method described above, we start by examining the time evolution of an initially fully localized magnon wave packet at the center of a lattice initially at rest ($x_n = 0$ and $\dot{x}_n = 0$), with $\tau = 10^{0.5}$. In Fig. 2 we plot the time evolution of the wave-function profile $|\psi_n|^2$ and its respective lattice deformation $x_n - x_{n-1}$ for some representative values of magnetoelastic coupling χ . In the absence of magnon-lattice interaction ($\chi = 0$), we observe the magnon wave function spreading ballistically over the entire lattice, which remains static. The scenario is significantly modified when we consider the interaction between magnon and lattice. For weak magnetoelastic coupling, nondispersive breathing magnon modes emerge and propagate with constant velocity, while a fraction of the magnon wave radiates through the lattice [see Figs. 2(b) and 2(c)]. By following such propagating solitonlike wave-function profiles and their respective lattice deformations, we observe a spatial matching with a nonvanishing profile of mechanical deformations propagating along the time. This holding behavior is consistent with the correlated dynamics between the excitation and the lattice deformation [52–55], which here represent signatures of the magnon-polaron formation. Magnon-polaron modes become slower as we increase the magnetoelastic coupling. A strong enough coupling (nearly half the magnon bandwidth) induces a significant fraction of the magnetic excitation to remain trapped around its initial location [see Fig. 2(d)]. Such behavior is also characterized by a spatial matching between the spin-mode and lattice deformation distribution. Thus, we observe a high degree of cooperation between the underlying excitations as a signature of the hybridized magnon-polaron state.

To better understand this rich set of dynamical profiles, we explore the participation function for the magnon [55,56],

$$\xi(t) = \sum_n 1/|\psi_n(t)|^4, \quad (6)$$

and the lattice vibrations [55,57],

$$\Xi = \frac{\left(\sum_n (x_{n+1} - x_n)^2 + \frac{\dot{x}_n^2}{\tau^2}\right)^2}{\sum_n \left[\frac{(x_{n+1} - x_n)^2}{2} + \frac{(x_n - x_{n-1})^2}{2} + \frac{\dot{x}_n^2}{\tau^2}\right]^2}. \quad (7)$$

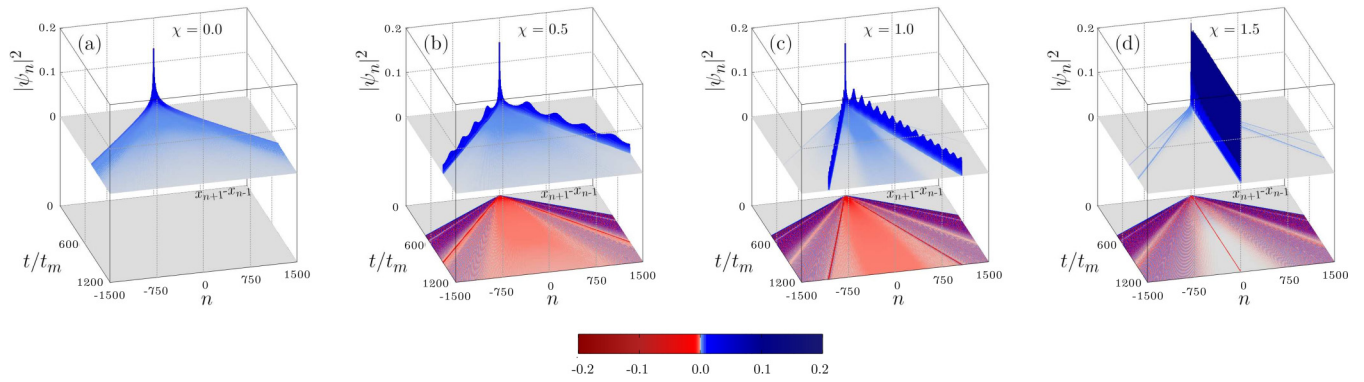


FIG. 2. Time evolution of the magnon wave function $|\psi_n|^2$ vs time and n ($n = 0$ represents the center of the chain). The local deformation $x_{n+1} - x_{n-1}$ of the chain is also investigated (see the density plots in the bottom parts). Calculations were done considering $\tau = 10^{0.5}$. (a) In the absence of magnon-lattice coupling ($\chi = 0.0$), the chain remains static and the magnon propagates ballistically along the chain (b),(c) considering $\chi = 0.5$ and 1 as the coupling between the lattice and the spin-waves promotes the appearance of a solitonlike mode traveling along the lattice. (d) For $\chi = 1.5$, the wave packet remains trapped around the center of the chain.

Such traditional quantities provide, respectively, an estimate of the number of lattice sites over which the magnon wave function is spreading at time t , and the number of disturbed lattice sites at time t . Their scaling behavior can be used to distinguish the different dynamical regimes. The asymptotic participation function becomes size-independent for localized wave packets. On the other hand, $\langle \xi(t \rightarrow \infty) \rangle \propto N$ and $\langle \Xi(t \rightarrow \infty) \rangle \propto N$ correspond to the regime where the magnon wave packet and the lattice vibrations are uniformly distributed over the lattice. In Fig. 3 we compute the long-time behavior of the participation function for the magnon [$\langle \xi(t \rightarrow \infty) \rangle$] and the lattice dynamics [$\langle \Xi(t \rightarrow \infty) \rangle$] versus the effective magnetoelastic coupling χ . Here, we explore the timescales of magnon and lattice vibrations. Calculations were done for $\tau = 10^{0.5}$ up to $10^{1.5}$. Magnon and lattice vibrations decrease the propagation as the magnetoelastic coupling increases. This aspect corroborates the previous scenario of magnon-polaron formation, characterized by nondispersive modes of spin and lattice vibrations exhibiting a constant velocity that decays as the magnetoelastic coupling increases. We further note the emergence of a kink singularity, which reveals an abrupt decrease at participation functions as χ increases even more. Such behavior signals the critical point that establishes the beginning of the stationary regime, corroborated by full agreement exhibited between the asymptotic dynamics of the magnon and the lattice vibrations. Furthermore, the long-time participation function is vanishingly small as the magnetoelastic coupling increases even more, i.e., the degree of trapping is enhanced. The critical magnetoelastic coupling increases as the $\tau = t_m/t_L$ grows, a consequence of the propagation of vibrational modes.

In Fig. 4(a), we display snapshots of the magnon wave packet and the corresponding lattice deformations for $\chi = 1.0$ and $\tau = 10^{0.5}$. In addition to magnon and lattice deformations exhibiting nondispersive modes with perfect spatial agreement, the lattice deformations are spreading over the lattice by developing wavefronts. With the magnon approximately as fast as the lattice dynamics, disturbances originating from the lattice wavefronts that extend along the tails inhibit the propagation of the magnon wave packet. Thus, a smaller coupling between magnetic and mechanical components is required for

the stationary formation of the magnon-polaron. This character is better understood when looking at Figs. 4(b) and 4(c), where we remain with $\chi = 1.0$, but we explore a range of τ . Figure 4(b) shows the wavefront velocity of the lattice deformations exhibiting a linear growth with τ . Figure 4(c)

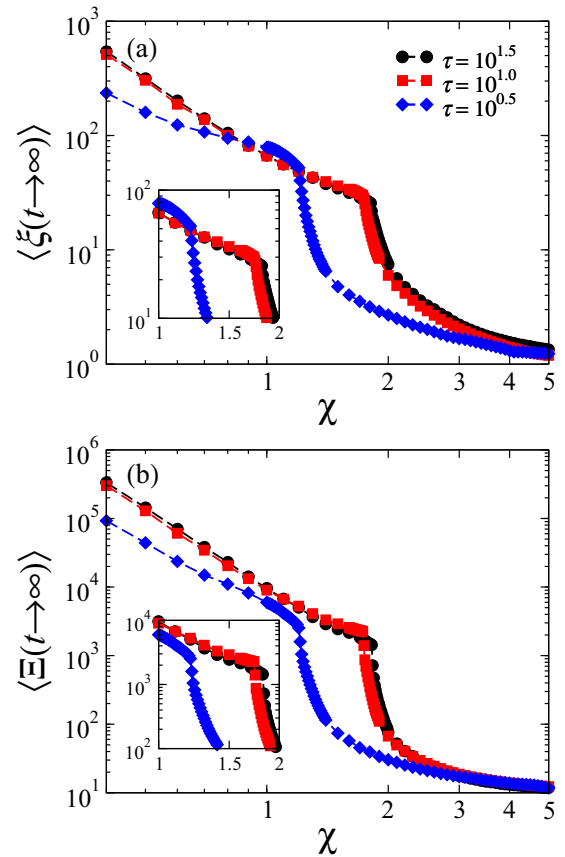


FIG. 3. Average participation function for both magnon and lattice vibrations at the long time limit vs χ , exploring $\tau = 10^{0.5}$ up to $10^{1.5}$. Data suggest a kink singularity developed at χ_c , above which the magnon-polaron formation stays stationary. Furthermore, such critical magnetoelastic coupling χ_c changes with different τ .

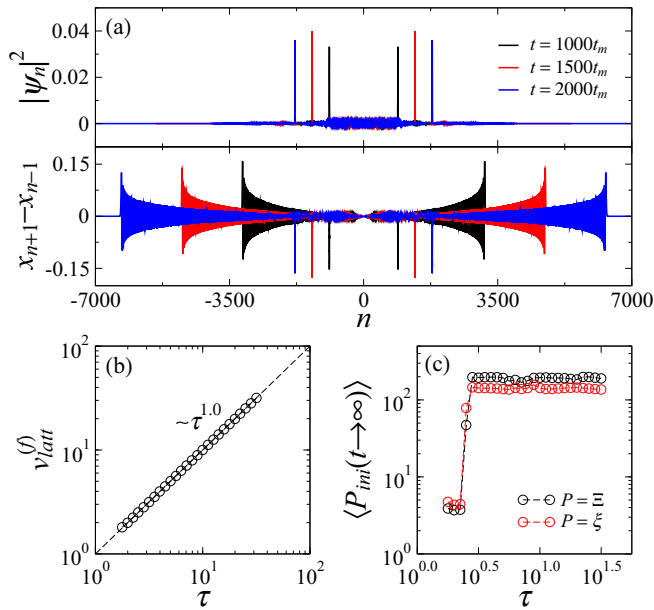


FIG. 4. With $\chi = 1.0$ and (a) $\tau = 10^{0.5}$, the spatial profile of the magnon wave function and lattice deformations describe the spatial matching and bound dynamics of the magnon-polaron formation, while (b) the wavefront velocity of the lattice vibrations vs τ shows a linear increase with τ . (c) The asymptotic participation functions around the initial magnetic excitation reveals a more pronounced spreading as τ increases. Thus, we observe that the lattice vibrations contribute to the magnon trapping and the consequent formation of a stationary magnon-polaron.

displays the asymptotic participation functions around the initial site of magnon excitation [$n_0 - 100 \leq n \leq n_0 + 100$]. A small ratio between the characteristic timescales of magnon and lattice vibration favors the stationary magnon-polaron formation, described by $\langle P_{\text{ini}}(t \rightarrow \infty) \rangle \approx 1$. With the magnon spreading slowly enough, the magnetoelastic coupling is unable to establish stationary formation.

We also explore the asymptotic regime of the return probabilities for the magnon and the lattice deformation:

$$R_0(t) = |\psi_{n=0}(t)|^2 \quad \text{and} \quad \rho_0(t) = |x_1(t) - x_{-1}(t)|. \quad (8)$$

Such measures offer the probability of finding the magnon wave packet or the lattice deformations at the position corresponding to the initial magnetic excitation. Thus, their scaling behaviors can also be used to distinguish between localized and delocalized wave packets in the long-time regime, with $R_0(t \rightarrow \infty) \rightarrow 0$ and $\rho_0(t \rightarrow \infty) \rightarrow 0$ connoting the magnon wave function and the lattice deformations escaping from its initial position, respectively. On the other hand, the return probability saturates at a finite value for a stationary regime of the magnon-polaron. We observe in Fig. 5 the asymptotic behavior of both return probabilities corroborating the previous results. For $\chi < \chi_c$, the magnon and the lattice deformations exhibit a vanishingly small return probability, which confirms a predominant spreading through the lattice. Above a critical magnetoelastic coupling, the asymptotic return probabilities become significantly larger than $1/N$. Allied to the monotonic growth of both return probabilities, such behavior reinforces the emerging self-trapping regime described

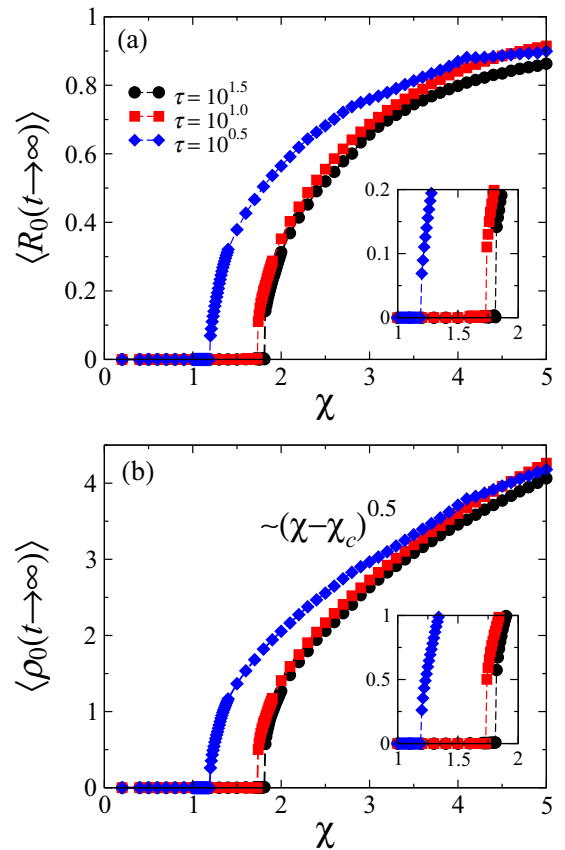


FIG. 5. The asymptotic return probabilities of (a) the magnon and (b) the lattice vibrations exhibit clear signatures of a phase transition between the traveling and stationary regimes of magnon-polaron formation, which corroborates the results shown in Fig. 3. Above the critical magnetoelastic coupling χ_c , magnon and lattice vibrations become significantly clustered around the site of the initial magnetic excitation.

earlier. Both quantities exhibit a trend $(\chi - \chi_c)^{0.5}$, and they confirm a dependence on the parameter τ (see the inset).

The magnon-polaron formation and its threshold between traveling and stationary regimes have also been identified by exploring the magnon-polaron velocity. For Fig. 6(a), we measure the mean velocity of the magnon-polaron modes at the long-time regime [$\langle v_{\text{tra}}(t \rightarrow \infty) \rangle$], and we investigate its relationship with χ . Data show the velocity decreasing as the effective magnetoelastic coupling increases, up to the threshold at which ($\chi \geq \chi_c$) vanishes. In addition to the critical magnetoelastic coupling showing full agreement with the measures of participation function (see Fig. 3) and return probability (see Fig. 5), the traveling velocity of the magnon-polaron decreases with $\langle v_{\text{tra}}(t \rightarrow \infty) \rangle \propto (\chi_c - \chi)^{0.5}$, the same exponent exhibited by the asymptotic return probability after the critical point.

To better understand such hybridized excitation of a magnon-polaron, in Figs. 6(b) and 6(c) we show profiles of the magnon wave function and the matching lattice deformation in a snapshot achieved during the time evolution for a system ruled by $\tau = 10^{0.5}$ and $\chi = 1.0, 1.5$. The magnon wave packet follows the standard solitonic profile $\text{sech}^2[\lambda(n + vt/t_m)]$ [9,10], either for the traveling [see Fig. 6(b)] or the

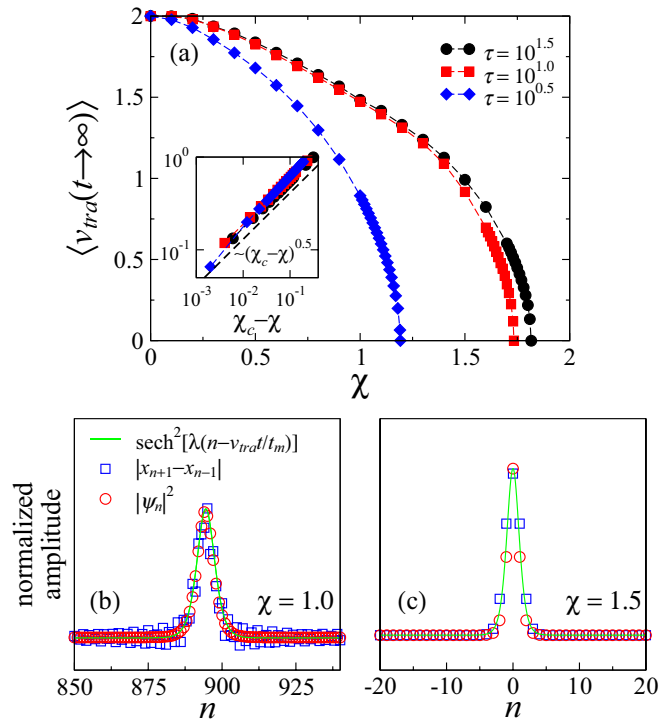


FIG. 6. The dynamics of the traveling formation of a magnon-polaron, with (a) the velocity vs χ and its respective scaling analysis. The best power-law fit provides $v \propto (\chi_c - \chi)^{1/2}$. The spatial profile of the magnon wave function and the matching lattice deformation for the magnon-polaron state, whether (b) traveling or (c) stationary, corroborates the characteristic spatial profile from the breathing bright solitons (fitting curves in solid lines).

stationary excitations [see Fig. 6(c)]. Such magnetic components are bound to a lattice structural kink that also exhibits the well-known breathing bright solitonlike spatial profile.

The consequences of different timescales of the magnetic and vibrational components are exhibited in Fig. 7, in which we extend our numerical experiments in order to offer a diagram of χ_c versus τ . For greater accuracy, data have been computed by analyzing the participation function, the return probability, as well as the magnon-polaron velocity. Systems in which the dynamics of magnons is comparable to the lattice dynamics show an increase in the critical magnetoelastic coupling χ_c as τ increases. However, when considering systems with an ever slower magnon dynamics, this behavior leads χ_c monotonically to a limit value that is on the order of half the magnon bandwidth [$\chi_c \approx 1.82(1)$]. Above this magnitude, no matter how much the lattice dynamics is faster than the magnon dynamics, the stationary magnon-polaron formation will be present. By analyzing the critical magnetoelastic coupling versus τ , the best fitting provides $\chi_c^{\text{lim}} \approx 1.825(5)$ and $(\chi_c^{\text{lim}} - \chi_c) \propto \tau^{-2}$ (see the inset).

IV. SUMMARY AND FINAL CONSIDERATIONS

In this work, we study how the lattice dynamics influences the dynamics of initially localized one-magnon excitations. We consider a quantum anisotropic Heisenberg ferromagnetic chain, in which the spins 1/2 belong to a chain of coupled

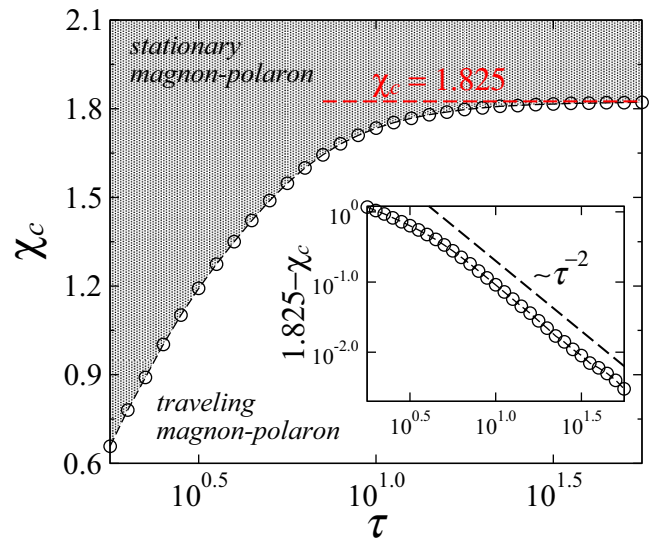


FIG. 7. Plot of χ_c vs τ phase diagram. Corroborating previous results, the magnetoelastic coupling necessary to the stationary formation of a magnon-polaron increases as τ grows. However, such behavior is restricted to the small enough τ regime. The continued increase in the ratio of characteristic timescales unveils a limit value χ_c^{lim} , above which the critical coupling becomes indifferent to τ . The best fitting is achieved for $\chi_c^{\text{lim}} = 1.825$ (on the order of half the magnon bandwidth).

harmonic oscillators. The magnon-elastic coupling was introduced by considering the longitudinal spin-spin exchange coupling as a linear function of the effective displacement between nearest-neighbor spins. By exploring the numerical solutions of the set of equations that govern the system, our results exhibit a framework for obtaining the magnon-polaron formation, features of which are ruled by effective magnetoelastic coupling. The characteristics of this hybridized state, with high cooperation between magnetic and mechanical components, are closely related to the magnetoelastic coupling. Weak enough couplings promote the formation of traveling magnon-polarons, the velocity of which depends on the strength of the magnetoelastic coupling. When analyzing stronger couplings, we are faced with a localization scenario in which the magnon-polaron formation remains trapped around the position of the initial magnetic excitation. This scenario was described by different physical quantities, such as the participation function, the probability of return, as well as the velocity of the traveling formation of a magnon-polaron. By exploring lattice and magnon characteristic timescales, we reveal that the critical magnetoelastic coupling that separates the stationary and traveling regimes is related to how much slower the magnon is compared with the lattice vibrations. The critical magnetoelastic coupling increases proportionally with the timescale of the magnon until a limit value is reached, above which the magnon dynamics no longer interferes at the coupling that can induce the stationary magnon-polaron. The current numerical results provide accurate estimates of the critical point and the respective singularities of the relevant quantities associated with the transition to the stationary regime. Although we focused our study on a single spin flip that is fully localized in lattices with open boundary

conditions, we claim that this same phenomenology extends to initially wide wave functions (such as Gaussian wave packets) as well as for periodic boundary conditions. Based on previous studies involving elastic lattices [58–60], propagating modes corresponding to the low-frequency region within a band of allowed energies are more susceptible to the aspects shown. Our study aims to contribute with the emergent development of a new class of ultrafast spintronic devices, and the consequent applications of a magnon-polaron. Considering that the present status of experiments with cold atoms trapped in optical lattices allows the study of Heisenberg XXZ and a fine control of a wide collection of anisotropies including the XX and XXX limits [24], we believe in the feasibility of the scheme proposed here. To conclude, it would be interesting

to have these results derived from an analytical framework, which would bring valuable new insights into the general dynamics involved in magnon-polaron formation. Future works that explore the solitonlike profile of magnon-polaron formation, such as coherence properties and binary collisions, may contribute to a better understanding and applicability.

ACKNOWLEDGMENTS

This work was partially supported by CAPES (Coordenação de Aperfeiçoamento de Pessoal do Nível Superior), CNPq (Conselho Nacional de Desenvolvimento Científico e Tecnológico), and FAPEAL (Fundação de Apoio à Pesquisa do Estado de Alagoas).

-
- [1] A. V. Chumak, A. A. Serga, and B. Hillebrands, *Nat. Commun.* **5**, 4700 (2014).
- [2] A. V. Chumak, V. Vasyuchka, A. Serga, and B. Hillebrands, *Nat. Phys.* **11**, 453 (2015).
- [3] V. Demidov, S. Urazhdin, G. de Loubens, O. Klein, V. Cros, A. Anane, and S. Demokritov, *Phys. Rep.* **673**, 1 (2017); magnetization oscillations and waves driven by pure spin currents.
- [4] J. Lan, W. Yu, R. Wu, and J. Xiao, *Phys. Rev. X* **5**, 041049 (2015).
- [5] D. Grundler, *Nat. Nanotechnol.* **11**, 407 (2016).
- [6] M. Krawczyk and D. Grundler, *J. Phys.: Condens. Matter* **26**, 123202 (2014).
- [7] B. Lenk, H. Ulrichs, F. Garbs, and M. Münzenberg, *Phys. Rep.* **507**, 107 (2011).
- [8] W. P. Su, J. R. Schrieffer, and A. J. Heeger, *Phys. Rev. Lett.* **42**, 1698 (1979).
- [9] T. Holstein, *Ann. Phys.* **8**, 325 (1959).
- [10] T. Holstein, *Ann. Phys.* **8**, 343 (1959).
- [11] C. Kittel and E. Abrahams, *Rev. Mod. Phys.* **25**, 233 (1953).
- [12] C. Kittel, *Phys. Rev.* **110**, 836 (1958).
- [13] M. I. Kaganov and V. M. Tsukernik, *J. Exp. Theor. Phys.* **9**, 151 (1959) [*Zh. Eksp. Teor. Fiz.* **36**, 224 (1959)].
- [14] P. Dai, H. Y. Hwang, J. Zhang, J. A. Fernandez-Baca, S.-W. Cheong, C. Kloc, Y. Tomioka, and Y. Tokura, *Phys. Rev. B* **61**, 9553 (2000).
- [15] P. Reutler, F. Moussa, M. Hennion, F. Wang, and A. Revcolevschi, *J. Magn. Magn. Mater.* **242-245**, 689 (2002); proceedings of the Joint European Magnetic Symposia (JEMS'01).
- [16] H. Man, Z. Shi, G. Xu, Y. Xu, X. Chen, S. Sullivan, J. Zhou, K. Xia, J. Shi, and P. Dai, *Phys. Rev. B* **96**, 100406(R) (2017).
- [17] J. Holanda, D. S. Maior, A. Azevedo, and S. M. Rezende, *Nat. Phys.* **14**, 500 (2018).
- [18] Y. Yahagi, B. Harteneck, S. Cabrini, and H. Schmidt, *Phys. Rev. B* **90**, 140405(R) (2014).
- [19] P. C. Lou, L. de Sousa Oliveira, C. Tang, A. Greaney, and S. Kumar, *Solid State Commun.* **283**, 37 (2018).
- [20] A. Milosavljević, A. Šolajić, J. Pešić, Y. Liu, C. Petrovic, N. Lazarević, and Z. V. Popović, *Phys. Rev. B* **98**, 104306 (2018).
- [21] F. Godejohann, A. V. Scherbakov, S. M. Kukhtaruk, A. N. Poddubny, D. D. Yaremkevich, M. Wang, A. Nadzeyka, D. R. Yakovlev, A. W. Rushforth, A. V. Akimov *et al.*, *Phys. Rev. B* **102**, 144438 (2020).
- [22] C. Berk, M. Jaris, W. Yang, S. Dhuey, S. Cabrini, and H. Schmidt, *Nat. Commun.* **10**, 2652 (2019).
- [23] S. Bao, Z. Cai, W. Si, W. Wang, X. Wang, Y. Shanguan, Z. Ma, Z.-Y. Dong, R. Kajimoto, K. Ikeuchi *et al.*, *Phys. Rev. B* **101**, 214419 (2020).
- [24] P. N. Jepsen, J. Amato-Grill, I. Dimitrova, W. W. Ho, E. Demler, and W. Ketterle, *Nature (London)* **588**, 403 (2020).
- [25] T. Yokouchi, S. Sugimoto, B. Rana, S. Seki, N. Ogawa, S. Kasai, and Y. Otani, *Nat. Nanotechnol.* **15**, 361 (2020).
- [26] X. Li, D. Labanowski, S. Salahuddin, and C. S. Lynch, *J. Appl. Phys.* **122**, 043904 (2017).
- [27] A. Rückriegel, P. Kopietz, D. A. Bozhko, A. A. Serga, and B. Hillebrands, *Phys. Rev. B* **89**, 184413 (2014).
- [28] N. Vidal-Silva, E. Aguilera, A. Roldán-Molina, R. A. Duine, and A. S. Nunez, *Phys. Rev. B* **102**, 104411 (2020).
- [29] P. Graczyk and M. Krawczyk, *Phys. Rev. B* **96**, 024407 (2017).
- [30] S. Zhang, G. Go, K.-J. Lee, and S. K. Kim, *Phys. Rev. Lett.* **124**, 147204 (2020).
- [31] K. Uchida, S. Takahashi, K. Harii, J. Ieda, W. Koshibae, K. Ando, S. Maekawa, and E. Saitoh, *Nature (London)* **455**, 778 (2008).
- [32] K. Uchida, J. Xiao, H. Adachi, J. Ohe, S. Takahashi, J. Ieda, T. Ota, Y. Kajiwara, H. Umezawa, H. Kawai *et al.*, *Nat. Mater.* **9**, 894 (2010).
- [33] H. Adachi, K.-i. Uchida, E. Saitoh, J.-i. Ohe, S. Takahashi, and S. Maekawa, *Appl. Phys. Lett.* **97**, 252506 (2010).
- [34] D. A. Bozhko, P. Clausen, G. A. Melkov, V. S. L'vov, A. Pomyalov, V. I. Vasyuchka, A. V. Chumak, B. Hillebrands, and A. A. Serga, *Phys. Rev. Lett.* **118**, 237201 (2017).
- [35] D. A. Bozhko, V. I. Vasyuchka, A. V. Chumak, and A. A. Serga, *Low Temp. Phys.* **46**, 383 (2020).
- [36] W. Jin, H. H. Kim, Z. Ye, S. Li, P. Rezaie, F. Diaz, S. Siddiq, E. Wauer, B. Yang, C. Li *et al.*, *Nat. Commun.* **9**, 5122 (2018).
- [37] H. J. Qin, K. Zakeri, A. Ernst, L. M. Sandratskii, P. Buczek, A. Marmodoro, T. H. Chuang, Y. Zhang, and J. Kirschner, *Nat. Commun.* **6**, 6126 (2015).
- [38] H. J. Qin, S. Tsurkan, A. Ernst, and K. Zakeri, *Phys. Rev. Lett.* **123**, 257202 (2019).
- [39] M. L. M. Laliou, R. Lavrijsen, R. A. Duine, and B. Koopmans, *Phys. Rev. B* **99**, 184439 (2019).
- [40] R. Kryshtal and A. Medved, *J. Magn. Magn. Mater.* **426**, 666 (2017).

- [41] N. K. P. Babu, A. Trzaskowska, P. Graczyk, G. Centała, S. Mieszczak, H. Głowiński, M. Zdunek, S. Mielcarek, and J. W. Kłos, *Nano Lett.* **21**, 946 (2021).
- [42] C. L. Chang, S. Mieszczak, M. Zelent, V. Besse, U. Martens, R. R. Tamming, J. Janusonis, P. Graczyk, M. Münzenberg, J. W. Kłos, and R. I. Tobey, *Phys. Rev. Applied* **10**, 064051 (2018).
- [43] D. Bloch, *J. Phys. Chem. Solids* **27**, 881 (1966).
- [44] I. K. Kamilov and K. K. Aliev, *Phys. Usp.* **41**, 865 (1998).
- [45] S. Streib, N. Vidal-Silva, K. Shen, and G. E. W. Bauer, *Phys. Rev. B* **99**, 184442 (2019).
- [46] R. Schmidt, F. Wilken, T. S. Nunner, and P. W. Brouwer, *Phys. Rev. B* **98**, 134421 (2018).
- [47] T. A. L. Ziman, *Phys. Rev. Lett.* **49**, 337 (1982).
- [48] S. Evangelou and D. Katsanos, *Phys. Lett. A* **164**, 456 (1992).
- [49] R. P. A. Lima, M. L. Lyra, E. M. Nascimento, and A. D. de Jesus, *Phys. Rev. B* **65**, 104416 (2002).
- [50] H. Liu, C. Zhang, H. Malissa, M. Groesbeck, M. Kavand, R. McLaughlin, S. Jamali, J. Hao, D. Sun, R. A. Davidson *et al.*, *Nat. Mater.* **17**, 308 (2018).
- [51] A. A. Serga, A. V. Chumak, and B. Hillebrands, *J. Phys. D* **43**, 264002 (2010).
- [52] A. Johansson and S. Stafström, *Phys. Rev. Lett.* **86**, 3602 (2001).
- [53] E. Mozafari and S. Stafström, *J. Chem. Phys.* **138**, 184104 (2013).
- [54] J.-y. Fu, J.-f. Ren, X.-j. Liu, D.-s. Liu, and S.-j. Xie, *Phys. Rev. B* **73**, 195401 (2006).
- [55] H. Nazareno and P. de Brito, *Phys. B* **494**, 1 (2016).
- [56] W. S. Dias, E. M. Nascimento, F. A. B. F. de Moura, and M. L. Lyra, *J. Magn. Magn. Mater.* **321**, 2304 (2009).
- [57] S. S. de Albuquerque, J. L. L. dos Santos, F. A. B. F. de Moura, and M. L. Lyra, *J. Phys.: Condens. Matter* **27**, 175401 (2015).
- [58] H. Matsuda and K. Ishii, *Prog. Theor. Phys. Suppl.* **45**, 56 (1970).
- [59] K. Ishii, *Prog. Theor. Phys. Suppl.* **53**, 77 (1973).
- [60] F. A. B. F. de Moura, M. D. Coutinho-Filho, E. P. Raposo, and M. L. Lyra, *Phys. Rev. B* **68**, 012202 (2003).